Proceedings of the 3rd IASME/WSEAS Int. Conf. on HEAT TRANSFER, THERMAL ENGINEERING AND ENVIRONMENT, Corfu, Greece, August 20-22, 2005 (pp338-343)

Numerical Simulations of Turbulent, Two-Phase Flows in Complex Geometries

M. AFSHAR
Department of Energy Engineering
Petroleum University of Technology
Khosro Jonoubi St., Sattar Khan St.
TEHRAN, IRAN
mafshar@put.ac.ir

Abstract: In this paper a new model for numerical simulation of two-phase flows in complex geometries is presented which is the first step in developing numerical simulation models for boiling heat transfer in complex geometries. The complexity of turbulence and two-phase flows exists in this problem and therefore, logical, convenient simplifications were made to solve the problem. A finite-volume based finite-element model is developed which resolved the difficulties for solving turbulent, single-phase flows in complex geometries. Also, a modified k-ε model is utilized for the solution of turbulent, two-phase bubbly flows. Since in many industrial applications, the flow is fully-developed, this problem is solved for this region. Considering the complexity of the problem, the results generated by numerical simulation are encouraging, and follow the data obtained in the corresponding experimental investigation of bubbly two-phase flows. Nevertheless, much effort is needed in modeling and numerical simulation methods to develop a sophisticated industrial tool.

Key-words: Two-phase flow, Turbulent, CVFEM, FVM, Numerical Simulation, Bubbly Flow

1 Introduction

Turbulent, two-phase flows exist in many industries, especially in process industries. There are many uncertainties in the mathematical modeling of these flows, Lahey [1], Carey [2], Drew and Wallis [3], and Whalley [4]. However, the mathematical models of dilute bubbly gas-liquid flows are reasonably well-established, relative to models for other two-phase gas-liquid flow patterns [1-4]. Though, they still suffer from difficulties, especially with regard to modeling of turbulence, interfacial terms, and in near-wall regions.

Attention here is focused on fully-developed, turbulent, upward, dilute, bubbly, gas-liquid two-phase flows, in straight ducts of triangular cross-section. A two-time-scale k-ε model has been proposed by Lopez de Bertodano et al. [7-9], in which an additional differential transport equation is used for the bubble-induced turbulence kinetic energy, and the shear-induced k-ε equations do not contain or need any extra sources for modeling bubble interactions with flow turbulence. They combined the two-time scale k-ε model [9] and an algebraic stress model developed by Naot and Rodi [10] for simulations of such flows. However, these simulations were carried out with the duct cross-section approximated as a circular sector, rather than a triangle, relatively coarse cylindrical-polar grids were used to disretize the duct cross-section, without any rigorous grid-independence checks. Also, a three-dimensional parabolic formulation to march the computations from the inlet plane of the duct to the fully-developed region is used.

In this work, the explicit algebraic stress model (EASM) of Gatski and Speziale [11] for single-phase turbulent flows is extended to make it applicable the fully-developed two-phase flows of interest, by incorporating key ideas of the two-time scale k-ε model of Lopez de Bertodano et al. [7-9]. The overall mathematical model, specialized to the fully-developed region [12], is solved using suitable adaptations of a two-dimensional control-volume finite element method (CVFEM) [13].

Considering that the proposed CVFEM allowed simulations in true triangular duct cross-sections, with extensive grid-independence checks, and without any unnecessary intrinsic grid bias, as that in the simulations of Lopez de Bertodano et al. [8,9], the results presented in this paper allow an accurate assessment of the predictive capabilities of the aforementioned mathematical model.

2 Mathematical Model

2.1 Governing Equations and Related Assumptions

For the gas-liquid bubbly two-phase flows considered here, the governing continuity and momentum equations can be written in the following forms [12]:

Gas-Phase Continuity Equation:

$$\nabla.(\alpha\rho_g V_g) = 0 \qquad \textbf{(1)}$$

Liquid-Phase Continuity Equation:

$$\nabla.\left[(1-\alpha)\rho_l V_l\right] = 0 \qquad \textbf{(2)}$$

Gas-Phase Momentum Equation:

$$0 = -\alpha\nabla p_g + \alpha\rho_g g + M_g \qquad \textbf{(3)}$$

Liquid-Phase Momentum Equation:

$$\nabla.\left[(1-\alpha)\rho_l V_l V_l\right] = -(1-\alpha)\nabla p_l + \nabla.\left[(1-\alpha)(\tau_1 + \tau_1^t)\right] + M_1 + (p_{il} - p_l)\nabla(1-\alpha) + (1-\alpha)\rho_l g \qquad \textbf{(4)}$$

where subscripts l and g refer to the liquid and gas phases, respectively, and, for convenience, α is used to denote the gas-phase void fraction, and (1-α) is the liquid-phase void fraction. Here, ρ, p, p_i are the phasic density, pressure, and pressure at the interface, respectively. V and τ are the mass weighted velocity and viscous stress tensor, respectively. g, M, and $\tau^t = -\rho_k \overline{V_k' V_k'}$ are the gravitational acceleration, the resultant interfacial force, and the turbulent, or Reynolds, stress tensor, respectively.

Considering the relatively small values of the gas-phase density and viscosity, in comparison to the corresponding values for the liquid phase, the advection terms $\nabla.(\alpha\rho_g V_g V_g)$, the stress tensor terms $(\tau_g + \tau_g^t)$ and, also, the $(p_{ig} - p_g)$ terms have been neglected in the gas-phase momentum equation, following the suggestions of Lance and Lopez de Bertodano [6], and Ellul and Issa [14]. It is assumed that the properties of the liquid and gas phases remain constant in the fully-developed region, and that the bubbles are essentially spherical with uniform diameter (5mm). Also, since attention is restricted to dilute two-phase flows, the bubbles do not coalesce or break up [12].

2.2 Interfacial Forces and Reynolds Stresses

The interfacial force is customarily divided into several components. Here, following Lahey et al. [15] and Oliveira [16], it is assumed that the dominant interfacial forces for the dilute, gas-liquid, bubbly two-phase flows of interest are the drag and lift forces. Thus,

$$M_l = M_l^D + M_l^L \qquad \textbf{(5)}$$

In this work, the drag force (per unit volume) is calculated using the following expression proposed by Ishii and Mishima [17]:

$$M_l^D = \frac{3}{8}\alpha\rho_l \frac{C_D}{R_b} V_r |V_r| \qquad \textbf{(6)}$$

where V_r=V_g-V_l is the relative velocity, R_b is the bubble radius, and C_D is the drag coefficient which is obtained using the following expression:

$$C_D = \frac{24}{\mathrm{Re}_b}(1 + 0.1\mathrm{Re}_b^{0.75}) \qquad \textbf{(7)}$$

Where

$$\mathrm{Re}_b = \frac{D_b \rho_l |V_r|}{\mu_m} \quad , \quad \mu_m = \frac{\mu_l}{(1-\alpha)} \qquad \textbf{(8)}$$

μ_m is the mixture viscosity, and D_b is the bubble diameter (= $2R_b$). The average lift force exerted by a rotational inviscid flow on a sphere, as derived by Drew and Lahey [18], is used for M_l^L:

$$M_l^L = C_L \alpha\rho V_r \times (\nabla \times V_1) \qquad \textbf{(9)}$$

where C_L is the lift coefficient and ranges from about 0.05 to 0.5, according to Lahey et al. [16]. The results presented in this paper correspond to C_L =0.1.

Following Lance and Bataille [19], it is assumed that (p_{il} – p_l) = 0. Furthermore, noting that ρ_g << ρ_l and neglecting surface tension, p_g = p_l.

To consider the effects of turbulence on interfacial terms, an approach proposed by Lopez de Bertodano [9] which consists of modeling the effects of turbulence by a turbulent dispersion force expressed as:

$$M_l^{TD} = C_{TD}\rho_l k_{SI} \nabla\alpha \qquad \textbf{(10)}$$

where k_{SI} is the shear-induced kinetic energy of turbulence in the liquid phase, and C_{TD} = 0.1, is used ($M_l = M_l^D + M_l^L + M_l^{TD}$).

Following Lopez de Bertodano et al. [7-9], the total turbulent kinetic energy of bubbly two-phase flow is:

$$k = k_{SI} + k_{BI} \qquad \textbf{(11)}$$

where k_{SI} and k_{BI} are the shear-induced and the bubble-induced turbulence terms, respectively. The transport equation for k_{SI} is:

$$\nabla\left[\rho_1(1-\alpha)V_1 k_{SI}\right] = \qquad \textbf{(12)}$$

$$\nabla.\left[(1-\alpha)\left(\mu_l + \frac{\mu_t}{\sigma_k}\right)\nabla(k_{SI})\right] + \rho_1(1-\alpha)(P_{SI} - \varepsilon_{SI})$$

where σ_k = 1.0, P_{SI} is the volumetric rate of production of shear-induced turbulent kinetic energy, and ε_{SI} is its dissipation rate [12].

Following the recommendations of Arnold et al. [20] and Lopez de Bertodano et al. [7,9],

$$k_{BI} = k_{BIa} = \frac{1}{2}\alpha C_{VM}\left|V_r\right|^2 \qquad \textbf{(13)}$$

where C_{VM} = 0.5, and k_{BIa} is the k_{BI} asymptotic value.

The ε_{SI} values are obtained as follows [12]:

$$\nabla.[\rho_l(1-\alpha)V_l\varepsilon_{SI}] = \nabla\left[(1-\alpha)\left(\mu_l + \frac{\mu_t}{\sigma_{\varepsilon SI}}\right)\nabla(\varepsilon_{SI})\right] + \rho_l(1-\alpha)\left(c_{\varepsilon 1}\frac{\varepsilon_{SI}}{k_{SI}}P_{SI} - c_{\varepsilon 2}\frac{{\varepsilon_{SI}}^2}{k_{SI}}\right) \qquad \textbf{(14)}$$

where $c_{\varepsilon 1}$ = 1.44, $c_{\varepsilon 2}$ = 1.92, and $\sigma_{\varepsilon SI}$ = 1.3.

The principle of linear superposition is also used for the two-phase Reynolds stress and turbulent viscosity [12]. Thus, using Cartesian tensorial notation,

$$\overline{u_i'u_j'} = \overline{(u_i'u_j')}_{SI} + \overline{(u_i'u_j')}_{BI} \qquad \textbf{(15)}$$

where the shear-induced (SI) components are obtained from the following equation:

$$\overline{(u_i'u_j')}_{SI} = 2k_{SI}b_{ij} + \frac{2}{3}k_{SI}\delta_{ij} \qquad \textbf{(16)}$$

For the EASM of Gatski and Speziale [17], Afshar [12] has shown that the b_{ij} term can be written as follows:

$$2b_{ij} = -\frac{\nu_t}{k}\overline{S}_{ij} + c_1\frac{\nu_t}{\varepsilon}(\overline{S}_{ik}\overline{S}_{jk} - 1/3\overline{S}_{kl}\overline{S}_{kl}\delta_{ij}) + c_2\frac{\nu_t}{\varepsilon}(\overline{\Omega}_{ik}\overline{S}_{jk} + \overline{\Omega}_{jk}\overline{S}_{ik}) \qquad \textbf{(17)}$$

where c_1 = 0.0876 and c_2 = 0.0935; and $\overline{S}_{ij} = \frac{1}{2}\left(\frac{\partial u_i}{\partial x_j} + \frac{\partial u_j}{\partial x_i}\right)$ and $\overline{\Omega}_{ij} = \frac{1}{2}\left(\frac{\partial u_i}{\partial x_j} - \frac{\partial u_j}{\partial x_i}\right)$ are the symmetric and asymmetric parts of the strain-rate tensor, respectively. The bubble-induced components are obtained from this expression by Arnold et al. [20]:

$$\overline{(u_i'u_j')}_{BI} = \alpha\left[\frac{1}{20}V_rV_r + \frac{3}{20}\left|V_r\right|^2\delta_{ij}\right] \qquad \textbf{(18)}$$

In these equations, the turbulent eddy viscosity is obtained from the following expression:

$$\nu = \nu + \nu \qquad \textbf{(19)}$$

where

$$\nu = 1.2R_b\alpha\left|V_r\right| \qquad \nu = c_\mu\frac{k_{SI}^2}{\varepsilon_{SI}} \qquad \textbf{(20)}$$

c_μ is obtained from ref. [17].

2.3 Boundary Conditions

Due to the complexity of the physical phenomena in the near-wall region in turbulent, bubbly, two-phase gas-liquid flows, it is not practical to numerically solve differential mathematical models of these flows all the way to the wall. Therefore, in this work, the near-wall region is bridged by appropriate wall-functions [12,25]. Values of $\overline{(u_i'u_j')}_{SI}$, k_{BI}, $\overline{(u_i'u_j')}_{BI}$, and relative velocity components are calculated from algebraic expressions, and they do not require the specification of any additional boundary conditions [18]. After each sweep of the iterative solver, the calculated α distribution was adjusted to obtain a desired average value.

3 Numerical Method

An extended control-volume finite element method (CVFEM) was developed for the solution of the mathematical models of the flows of interest [5,12]. This CVFEM is based on a primitive-variables, co-located, equal-order formulation: it works directly with the velocity components, pressure, void fraction, and turbulence kinetic energy and its dissipation rate; and these dependent variables are stored at the same nodes and interpolated over the same triangular elements in the finite-element mesh [5].

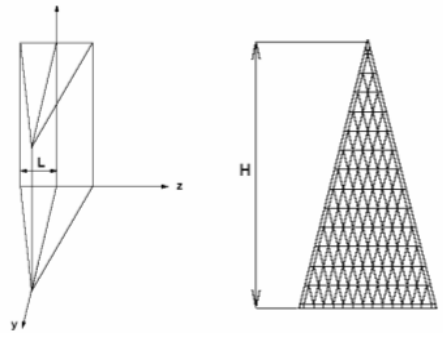

(a) (b)

Fig. 1: Fully-developed, gas-liquid, bubbly, turbulent, two-phase flows in a duct of triangular cross-section: (a) problem schematic and notation; (b) typical uniform finite-element discretization of the calculation domain.

Numerous preliminary computations, including grid refinement checks, were performed for the selected test problem. It was concluded that a 5922 triangular element grid, Fig. 1, was adequate for the final computations. In single-phase flow simulations, α = 0, this grid yielded numerical results that were within ±3%

of the corresponding grid-independent values, obtained using an extension of Richardson's extrapolation procedure [12].
The iterative solution procedure was stopped when the sums of the absolute values of the normalized residues in the w (axial velocity) and *p* sets of discretized equations, as well as the relative change in the value of the duct-center, or centroidal, axial velocity, were all individually less than 10^{-5}, and, in addition, the relative change in the calculated average void-fraction values in two successive iterations was less than, 10^{-4}.

4 Results

4.1 Single-Phase Flow

Axial velocity profiles along the duct cross-section center-line, z = 0 in Fig. 1, along with the experimental data of Lopez de Bertodano [9], are shown in Fig. 2; and the corresponding results along a line parallel to the *z* axis, at *y* = 0.03 m, are shown in Fig. 3. The results are in good agreement with the experimental data, except near the triangle vertex (*y*/H = 1), where the predicted results are lower than the experimental data.

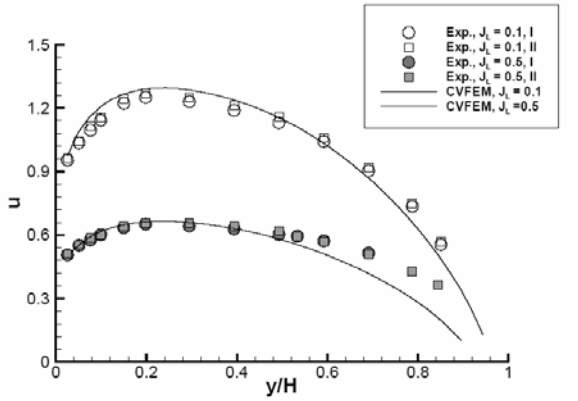

Fig. 2: Liquid-phase axial velocity (u_l in m/s) profiles along the line z = 0 m, for $<\alpha> = 0$.

The near-wall regions were bridged by using wall-functions, therefore, the last node in the internal computational domain for the J_L = 1 m/s test case is physically closer to wall than the J_L = 0.5 m/s test case. particularly in the vicinity of the vertex of the triangular duct cross-section.
The results in Fig. 3, along the line parallel to *z*-axis at *y* = 0.03 cm, are in excellent agreement with the experimental results of Lopez de Bertodano (1992):

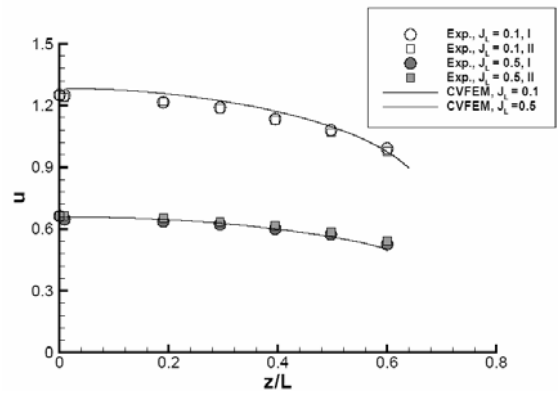

Fig. 3: Liquid-phase axial velocity (u_l in m/s) profiles along the line y = 0.03 m, for $<\alpha> = 0$.

Along this particular line, the predicted velocities are not directly affected by the wall-function approximations in the vicinity of the triangular cross-section vertex.

4.2 Two-Phase Flow

The results obtained in the single-phase flow simulations were used as starting values for the two-phase flow simulations, and the average void fraction was increased in three steps from zero (single-phase flow) to the desired value, obtained by numerical integration of local experimental void-fraction values [9,12].
The liquid-phase axial velocity and the void-fraction profiles along the center line of the duct (*z* = 0) are shown, respectively, in Figs. 4 and 5 for J_L = 1.0 m/s, for three nominal average void-fraction values, along with the experimental data of Lopez de Bertodano [9]; and the corresponding results for J_L = 0.50 m/s are shown in Figs. 6 and 7. The axial velocity profiles overpredict the experimental data near the bottom wall of the triangular cross-section, and underpredict them close to the vertex. One of the causes of the latter discrepancy, as was mentioned for the corresponding single-phase ($<\alpha>=0$) numerical predictions, is the relatively sharp acute vertex angle, and the associated large distance of the near-wall node from the vertex. Again, as was explained in the context of single-phase flow results, the underpredictions of the experimental data are larger for the results obtained for lower liquid-phase superficial velocity (Fig. 6, J_L = 0.5 m/s), since, for this case, the near-wall region is larger than that for J_L = 1 m/s.
As shown in Figs. 5 and 7, the experimental data indicates that void-fraction peaking occurs in the vicinity of the bottom wall, and, then, the void-fraction values decrease away from this wall, followed by a region of almost constant void fraction in the central

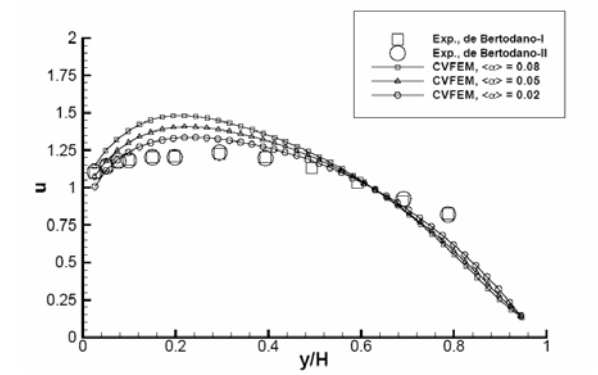

Fig. 4: Liquid-phase axial velocity (u_1 in m/s) profiles along the line z = 0 m, for J_L = 1.0 m/s.

regions of the duct, and, finally, the void-fraction values increase again, close to the vertex of the triangular cross-section. The numerically predicted void-fraction profiles follow the same general pattern as that of the experimental data: peaking of the void fraction values occurs in the region close to the bottom wall. However, they deviate from the experimental data, in the location, and also in the magnitude, of the peak (highest) void-fraction value in this region.

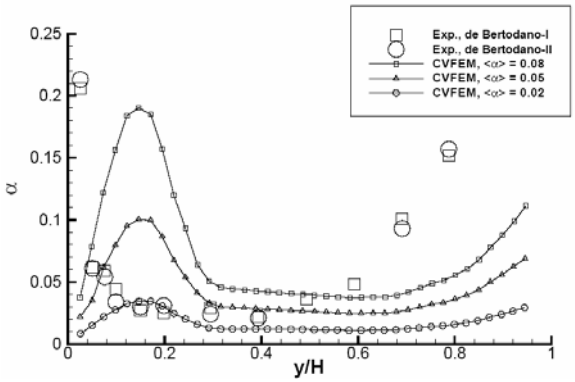

Fig. 5: Void fraction profiles along the line z = 0 m for J_L = 1.0 m/s.

In the near-wall regions, there are extra interfacial forces which affect, in particular, the bubble distributions in this area, as indicated in the published works of Marie et al. [22] and Antal et al. [23]. The inaccurate predictions of the void peaking in a location which is displaced in comparison to experimental data also affects the liquid-phase axial velocity profiles in this region. The drag force, between the liquid and bubbles, increases with the increase in void-fraction values in this region, and, hence, increases the numerically predicted liquid-phase axial velocity, as shown in Figs. 4 and 6. The numerical void-fraction values in the region near the vertex underpredict the experimental results. Unfortunately, no

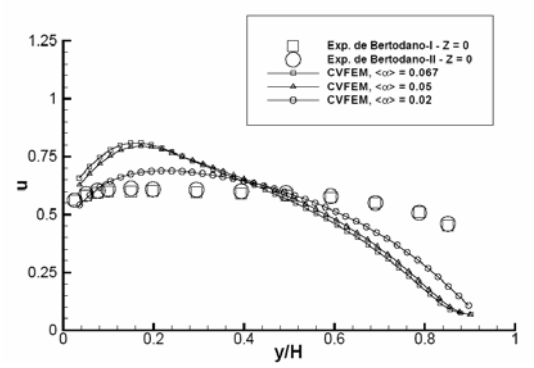

Fig. 6: Liquid-phase axial velocity (u_1 in m/s) profiles along the line z = 0 m, for J_L = 0.5 m/s.

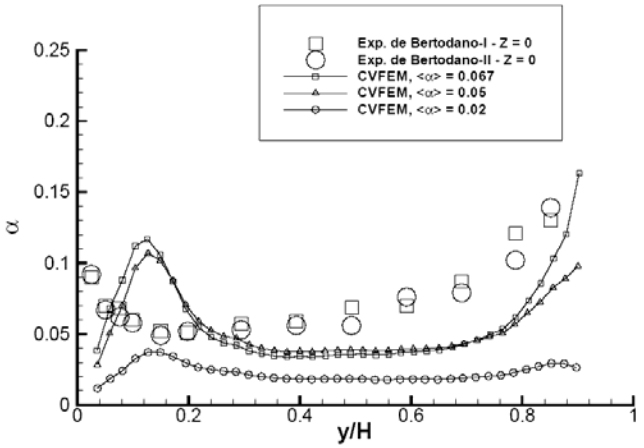

Fig. 7: Void fraction profiles along the line z = 0 m for J_L = 0.5 m/s.

tabulations of experimental results for the liquid- or gas-phase secondary velocities in the duct are provided by Lopez de Bertodano [9], which would have facilitated an analysis of this particular underprediction of the experimental data. Nevertheless, it seems reasonable to assume that the bridging of a relatively large near-wall region close to the vertex by wall-functions has contributed to this disagreement between numerical predictions and experimental results.

6 Summary

In this work, numerical predictions of fully-developed, turbulent, dilute, bubbly gas-liquid two-phase flows in a vertical duct with an isosceles triangular cross-section were presented. A two-fluid model was used. The turbulence terms were modeled using an extension of an algebraic stress model [5, 11], incorporating key ideas of a two-time scale $k-\varepsilon$ model [7-9]. Wall functions were

used to bridge the near-wall regions [24]. This mathematical model of the flows of interest was solved directly in the fully-developed region, for the first time, using an extended two-dimensional CVFEM [5,12].

The results obtained agree qualitatively with the experimental data of Lopez de Bertodano et al. [7-9]. However, this investigation shows the need for much more research to develop better models for these flows in noncircular ducts. In particular, development of closure models for the turbulence terms and the interfacial forces, especially in the vicinity of the walls.

References :

[1] R.T. Lahey, The Analysis of Phase Separation and Phase Distribution Phenomena Using Two-Fluid Models, *Nuclear Eng. & Design*, vol. 122, pp. 17-40, 1990.

[2] V.P. Carey, *Liquid-Vapor Phase-Change Phenomena*, Hemisphere, Washington D.C., 1992.

[3] D.A. Drew and G.B. Wallis, Fundamentals of Two-Phase Flow Modeling, *Proc. 3rd. Int. Workshop on Two-Phase Flow Fundamentals*, Imperial College, 1992.

[4] P.B. Whalley, *Two-Phase Flow and Heat Transfer*, Oxford Science Publications, Oxford University Press, Oxford, 1996.

[5] M. Afshar, Comparative Evaluation of Four Turbulence Models For Fully-Developed, Turbulent Flows in Straight Ducts of Arbitrary Cross-Sections, *Proceedings of the 8th CFD conference of Canada*, Montreal, Canada, June 11-13, 2000.

[6] M. Lance and M. Lopez de Bertodano, Phase Distribution and Wall Effects in Bubbly Two-Phase Flows, *Proc. 3rd. Int. Workshop on Two-Phase Flow Fundamentals*, Imperial College, London, 1992.

[7] M. Lopez de Bertodano, R.T. Lahey, and O.C. Jones, Development of a $k-\alpha$ Model for Bubbly Two-Phase Flow, *Trans. ASME, J. Fluids Eng.*, vol. 116, pp. 128-134, 1994.

[8] M. Lopez de Bertodano, R.T. Lahey, and O.C. Jones, Phase Distribution in Bubbly Two-Phase Flow in Vertical Ducts, *Int. J. Multiphase Flow*, vol. 20, pp. 805-818, 1994.

[9] M. Lopez de Bertodano, *Turbulent Bubbly Two-Phase Flow in a Triangular Duct,* Ph.D. Thesis, Rensselaer Polytechnic Institute, Troy, USA, 1992.

[10] D. Naot and W. Rodi, Calculation of Secondary Currents in Channel Flow, Proc. American Soc. *Civil Engineers*, vol. 108, pp. 948-968, 1982.

[11] T.B. Gatski and C.G. Speziale, On Explicit Algebraic Stress Models for Complex Turbulent Flows, *J. Fluid Mech.*, vol. 254, pp. 59-78, 1993.

[12] M. Afshar, *Numerical Predictions of Fully-Developed, Turbulent, Single-Phase and Bubbly Two-Phase Flows in Straight Ducts,* Ph.D. thesis, McGill University, Montreal, Canada, 1998.

[13] B.R. Baliga, Control-Volume Finite Element Methods for Fluid Flow and Heat Transfer, in W.J. Minkowycz and E.M. Sparrow (ed.), *Advances in Numerical Heat Transfer, vol. 1, Chapter 3, Taylor & Francis*, Washington D.C., 1997.

[14] I.R. Ellul and R.I. Issa, Prediction of the Flow of Interspersed Gas and Liquid Phases Through Pipe Bends, *Chem. Eng. Res. Des.*, vol. 65, pp. 84-96, 1987.

[15] R.T. Lahey, M. Lopez de Bertodano, and O.C. Jones, Phase Distribution in Complex Geometry Conduits, Using Two-Fluid Models, *Nuclear Eng. & Design*, vol. 141, pp. 177-201, 1993.

[16] P.J. Oliveira, *Computer Modelling of Multidimensional Multiphase Flow and Application to T-Junctions, Ph.D thesis,* University of London, London, England, 1992.

[17] M. Ishii and K. Mishima, Two-Fluid Model and Hydrodynamic Constitutive Relations, *Nuclear Eng. & Design*, vol. 82, pp. 107-126, 1984.

[18] D.A. Drew and R.T. Lahey, The Virtual Mass and Lift Force on a Sphere in Rotating and Straining Flow, *Int. J. Multiphase Flow*, vol. 13, pp. 113-121, 1987.

[19] M. Lance and J. Bataille, Turbulence in the Liquid Phase of a Uniform Bubbly Air-Water Flow, *J. Fluid Mech.*, vol. 222, pp. 95-118, 1991.

[20] G.S. Arnold, D.A. Drew, and R.T. Lahey, Derivation of Constitutive Equations for Interfacial Forces and Reynolds Stress for a Suspension of Spheres Using Ensemble Averaging, *Chem. Eng. Communications*, vol. 86, pp. 43-54, 1988.

[21] Y. Sato, and K. Sekoguchi, Liquid Velocity Distribution in Two-Phase Bubbly Flow, *Int. J. Multiphase Flow*, vol. 2, pp. 79-95, 1975.

[22] J.L. Marie, E. Moursali, and S. Tran-Cong, Similarity Law and Turbulence Intensity Profiles in a Bubbly Boundary Layer at Low Void Fractions, *Int. J. Multiphase Flow*, vol. 23, pp. 227-247, 1997.

[23] S.P. Antal, R.T. Lahey, and J.E. Flaherty, Analysis of Phase Distribution in Fully-Developed Laminar Bubbly Two-Phase Flow, *Int. J. Multiphase Flow,* vol. 17, pp. 635-652, 1991.

[24] Afshar, M., Baliga, B.R., A Logarithmic Law of the Wall for Upward, Turbulent, Bubbly Two-Phase Flow, *Proceedings of the 2nd Int. Symposium on Turbulence, Heat and Mass Transfer*, Delft, the Netherlands, June 9-12, 1997.